Article:
Zhang, Y, Lou, D, Tan, P et al. (2 more authors) (2019) Emission reduction characteristics of a catalyzed continuously regenerating trap after-treatment system and its durability performance. Journal of Environmental Sciences, 84. pp. 166-173. ISSN 2336-1964

https://doi.org/10.1016/j.jes.2019.05.001

Emission reduction characteristics of a catalyzed continuously regenerating trap after-treatment system and its durability performance

Yunhua Zhang[1], Diming Lou[1,*], Piqiang Tan[1], Zhiyuan Hu[1], Hu Li[2]

1. School of Automotive studies, Tongji University, Shanghai 201804, China
2. School of Chemical and Process Engineering, Faculty of Engineering, University of Leeds, Leeds LS2 9JT, UK

Abstract: The primary purpose of this study was to investigate the effect of a catalyzed continuously regenerating trap (CCRT) system composed of a diesel oxidation catalyst (DOC) and a catalyzed diesel particulate filter (CDPF) on the main gaseous and particulate emissions from an urban diesel bus, as well as the durability performance of the CCRT system. Experiments were conducted based on a heavy chassis dynamometer, and a laboratory activity test as well as X-ray photoelectron spectroscopy (XPS) test were applied to evaluate the changes of the aged CCRT catalyst. Results showed that the CCRT could reduce the CO by 71.5% and the total hydrocarbons (THC) by 88.9%, and meanwhile promote the oxidation of NO. However, the conversion rates for CO and THC dropped to 25.1% and 55.1%, respectively, after the CCRT was used for one year (~ 60,000 km), and the NO oxidation was also weakened. For particulate emissions, the CCRT could reduce 97.4% of the particle mass (PM) and almost 100% of the particle number (PN). The aging of the CCRT resulted in a reduced PM trapping efficiency but had no observable effect on the PN; however, it increased the proportion of nucleation mode particles. The activity test results indicated that the deterioration of the CCRT was directly relevant to the increase in the light-off temperatures of the catalyst for CO, C_3H_8 and NO_2. In addition, the decreased concentrations of the active components Pt^{2+} and Pt^{4+} in the catalyst are also important factors in the CCRT deterioration.

Keywords:
Diesel bus
Catalyzed continuously regenerating trap (CCRT)
Emissions
Durability
Deterioration

---

* Corresponding author. E-mail: loudiming@tongji.edu.cn (Diming Lou)

Introduction

Diesel engines have been widely used in heavy-duty vehicles, especially in urban buses and trucks throughout the world for their strong power, good economy and high reliability (Liu et al., 2017; Shen et al., 2018). However, they emit a huge amount of particulates and nitrogen oxide (NO_x), which not only pollute the atmospheric environment but also endanger human health. Thus, emission regulations are continuously being introduced to limit the particulate and NO_x emissions from diesel engines (Shen et al., 2015; Jung et al., 2017). To meet the increasing emission regulations, exhaust after-treatment equipment is necessary for diesel engines (Guardiola et al., 2017; Fleischman et al., 2018), among which the diesel oxidation catalyst (DOC) and catalyzed diesel particulate filter (CDPF) are indispensable in emission control (He et al., 2015; Zhang et al., 2018a). The DOC can not only remove the CO and hydrocarbons (HC) emissions, but also oxidize the NO to NO_2, and a higher ratio of NO_2 to NO_x is beneficial to the combustion of the trapped soot in the CDPF (Guan et al., 2015; Zhang et al., 2018b). The catalyzed continuously regenerating trap (CCRT), consisting of a DOC and a CDPF, can reduce the CO and HC by more than 60%, as well as remove more than 90% of the particulate emissions of diesel engines (Caliskan and Mori, 2017; Orihuela et al., 2018). However, it is difficult to maintain a CCRT's high efficiency during its whole life cycle, because the catalyst of the CCRT will undergo aging phenomena due to high temperature, chemical poisoning, catalyst coking, clogging, etc., which will result in a decrease in CCRT performance and the eventual failure of CCRT regeneration (Gilpin et al., 2014). Available literature was investigated for durability assessment of after-treatment catalysts during aging. Zhang et al. (2018a) found that thermal aging was the main reason for the loss of catalytic activity of DOC based on an engine test bench. Lou et al. (2016) and Zhang et al. (2017) used a portable emission measurement system to investigate the durability performance of CCRT and found that the aging of the CCRT resulted in lower PN trapping efficiency, but the particle size distribution (PSD) was not studied. In terms of the aging mechanism of the after-treatment devices, Hauff et al. (2010) revealed that the durability performance of the aftertreatment catalyst depended on the its surface area, while Wiebenga et al. (2012) and Li et al. (2012) thought that durability performance of a CCRT can be characterized by the light-off performance of the catalyst. Auvray et al. (2013) and Honkanen et al. (2017) reported that the deterioration of the CCRT can be attributed to Pt/Pd sintering. Current studies mainly focus on the effect of CCRT durability on the emission reduction characteristics and its aging mechanism separately. In addition, most of the studies conducted laboratory aging evaluation

and real-world on-the-road aging evaluation separately. Consequently, it is necessary to conduct an integrated research study on the effect of durability on CCRT performance both from the viewpoint of the reduction efficiency for main pollutants, and by catalyst deterioration analysis using real-world test and laboratory analysis methods. In this paper, the effect of a CCRT system on the emissions of CO, total hydrocarbons (THC), NO/NO_2, particle mass (PM), particle number (PN) and PSD from an urban diesel bus, as well as the durability of this effect, were investigated. In addition, the changes in light-off performance and active elements were also investigated to evaluate the deterioration of the catalyst in the CCRT.

1 Materials and methods

1.1 Experimental materials

1.1.1 Test vehicle

The test vehicle used in this study is a 7.l L urban diesel bus meeting the China Ⅲ emission standard. The curb weight of the bus is 16,500 kg, and its maximum speed reaches 85 km/hr. The engine of this bus has a compression ratio of 18, and its rated power is 177 kW. And the maximum torque of this bus is 920 N·m. A CCRT after-treatment system was used to retrofit the bus to study its emission reduction performance as well as the durability performance.

1.1.2 CCRT specifications

The after-treatments used in this study were a new and an aged CCRT consisting of an upstream DOC and a downstream CDPF. The new and aged CCRTs had the same specifications presented in **Table 1**. Before the test, a real-world on-the-road de-greening of the new CCRT system was conducted for one week on the bus's regular route in order to activate the catalyst. Then the CCRT was considered as a fresh one for testing. The aging of the CCRT was also based on real-world on-the-road driving on the bus's regular route: the CCRT was operated on the bus for one year with mileage of about 60,000 km. This was used as the aged CCRT for testing.

1.2 Experimental procedure

1.2.1 Heavy chassis dynamometer test

1.2.1.1 Test bench

As shown in **Fig. 1**, the experimental system consists of a chassis dynamometer (ECDM 72H-2MOT, MAHA-AIP, Germany), a diesel bus, a CCRT after-treatment system, EchoStar SEMTECH-D (SEMTECH-D, Sensors, USA), an EEPS^{TM} engine exhaust particle sizer (EEPS, EEPS3090, TSI, USA), and a two-stage diluter (DI-2000, Dekati, Finland). The CO,

THC, and NO/NO_2 emissions were measured by the Sensors SEMTECH-D with test accuracy of ±2%, ±1% and ±2%, respectively. The particle number concentration and PSD with particle sizes ranging from 5.6 to 560 nm were measured by the TSI EEPS 3090.

1.2.1.2 Driving cycle

The driving cycle used in this study was the Chinese city bus cycle (CCBC); the whole CCBC duration was 1314 sec. Its mileage was about 5.897 km. The minimum and maximum speed was 0 and 60 km/hr, respectively, and the average speed was 16.2 km/hr, which can reflect the typical running characteristics of buses in China.

1.2.1.3 Test procedure

First, the gaseous and particulate emissions from the bus equipped with the fresh and aged CCRT systems, respectively, were measured based on the heavy-duty chassis dynamometer, as shown in **Fig. 1**. Both of the tests were repeated three times in order to reduce test error. Then catalyst samples with size of 20 mm × 40 mm (diameter × length) were cut from the central position of the fresh and aged DOCs and CDPFs, which were utilized to carry out activity evaluation tests and X-ray photoelectron spectroscopy (XPS) characterization experiments, aiming to evaluate the changes in the light-off performance and catalyst active components.

1.2.2 Catalytic activity evaluation

The catalytic activity of the fresh and aged CCRT catalyst samples was evaluated using the temperature-programmed reduction (TPR) method, and the test device (CHEMISORB 272, Micromeritics, USA) consisted of a gas supply unit, reaction unit and analysis unit, as shown in **Fig. 2**. The gas supply unit provided the CO, C_3H_8, NO, O_2 and N_2 components for study. The saturated vapor was supplied from the vapor feeder, and all the gases were mixed through the gas mixer. Then the mixed gas entered the temperature-programmed heating reactor. The catalyst sample including DOC and CDPF was put in the heating reactor, which was wrapped with asbestos, then Fourier transform infrared spectroscopy (FTIR) was used to analyze the performance of the catalysts. The reaction gas contained 400 ppm NO, 400 ppm C_3H_8, 400 ppm NO, 10% CO_2, 5% O_2, and 5% H_2O. While N_2 was used as a balance gas. The space velocity was set to 40000 hr^{-1}, and the temperature was increased at a controlled rate of 5 ◦C/min from 50◦C to 500◦C.

The conversion rates of CO and C_3H_8 and the NO_2 production rate were used to characterize the CCRT catalyst activity. The conversion rates were calculated by Eq. (1):

$$\eta = \frac{c_o - c}{c_o} \times 100\% \quad (1)$$

where η represents the CO and C_3H_8 conversion rates and NO_2 production rate, c_o and c (ppm) are the CO, C_3H_8 and NO concentrations of the feed gas and reactor outlet, respectively.

1.2.3 XPS evaluation

X-ray photoelectron spectroscopy evaluation was applied to analyze the changes in the concentration and valence distribution of the active element Pt in the aged CCRT catalyst. In this study, an X ray photoelectron spectrometer (PHI 5000C ESCA, PerkinElmer, USA) was used to analyze the active elements Pt^{2+} and Pt^{4+} on the surface of catalyst samples.

2 Results and discussion

2.1 Experimental result analysis

2.1.1 Exhaust temperatures and flow rates

Fig. 3 gives the evolution of the exhaust temperature, flow rate and speed of the bus during the CCBC driving cycle. It can be seen that the exhaust temperature and flow rate coincided with the speed of the bus. The exhaust temperature ranged from 132 to 345℃, and the average temperature throughout the CCBC was about 216℃. The exhaust flow rate had a distribution ranging from 0.39 to 6.49 m^3/min.

2.1.2 Gaseous emissions

Fig. 4a shows the CO emission rates of the bus with fresh and aged CCRT during the CCBC. The CO emission rate had a similar evolution to the exhaust flow rate, as well as the speed. After using the CCRT, the CO emission rate decreased significantly. Compared with the aged CCRT, the fresh one resulted in larger reduction in the CO emission. **Fig. 4b** gives the CO emission factors of the bus with the fresh and aged CCRTs. The CO emission factor of the bus without CCRT was 1.32 mg/km. When the bus used the fresh CCRT, the CO emission factor decreased by 71.5% and reached 0.38 mg/km. After using the aged CCRT, the CO emission factor fell to 0.98 mg/km with a decrease of 25.3% compared to that without CCRT. This is attributed to the thermal aging of the DOC working long hours in a high temperature environment, which not only leads to growth of noble metal particles, but also causes the carrier coating to sinter; this results in decreased activity on specific catalyst surfaces followed by activity deterioration (Luo et al., 2010; Johns et al., 2015).

Fig. 5a presents the THC emission rates of the bus with the fresh and aged CCRT during the CCBC. The THC emission rates coincided well with the exhaust flow rate, as well as the speed. The THC emission rate apparently decreased after using the CCRT. The fresh CCRT had a better THC reduction effect compared with the aged CCRT sample. The THC emission factors of the bus with fresh CCRT and aged CCRT are presented in **Fig. 5b**. The THC emission factor of the bus without CCRT was 0.26 mg/km. After using the fresh CCRT, the

THC emission factor decreased to 0.03 mg/km with a reduction of 88.9%. For the aged CCRT, a decrease of 55.1% in the THC emission was observed compared to the bus without CCRT. The main reason for the change is that thermal aging of the DOC results in the collapse of the catalyst structure and the noble metal embedded therein; then, the specific surface of the catalyst sample declines and causes decreased activity (Kolli et al., 2010; Kim et al., 2008).

The NO/NO_2 emission characteristics of the bus with fresh and aged CCRT during the CCBC are presented in **Fig. 6a**. It can be seen that the NO and NO_2 emission rates had similar trends with the exhaust flow rate, as well as the bus speed. The NO emission rate decreased slightly after using the CCRT, especially for the aged one. On the contrary, the use of CCRT increased the NO_2 emission rate compared to the bus without CCRT. The aging of the CCRT weakened its ability to oxidize NO to NO_2, and this is attributed to the reduced dispersion of the noble metal particles in CCRT caused by thermal aging of the catalyst (Matam et al., 2013).

Fig. 6b presents the NO and NO_2 emission factors of the bus with the fresh and aged CCRT. The emission factors of NO and NO_2 for the bus without CCRT were 8.54 and 0.91 g/km, respectively, and NO_2 accounted for 9.6% of the NO_x. After the bus was equipped with the fresh CCRT, the NO emission factor decreased to 8.00 g/km while the NO_2 emission factor increased to 1.62 g/km, and the proportion of NO_2 in NO_x was 16.9%. When the bus used the aged CCRT, the NO emission factor was 8.18 g/km, while the NO_2 emission factor was 1.44 g/km. The total NO_x is equivalent to that of the fresh CCRT, but the NO_2 proportion decreased to 15.0%.

2.1.3 Particulate emissions

Fig. 7 shows the PN concentration emission of the bus with the fresh and aged CCRT during the CCBC. The PN emission concentration of the bus without CCRT was distributed from 10^7 to 10^9 particles/cm^3. After using the CCRT, the PN emission concentration decreased by two orders of magnitude or more. The fresh CCRT outperformed the aged CCRT in terms of PN concentration reduction.

Fig. 8 presents the PN and PM emission factors of the bus with the fresh and aged CCRT. The PN emission factor of the bus without CCRT was 2.47×10^{14} particles/km. After using the fresh CCRT, the PN emission factor fell to 5.28×10^{11} particles/km with a decrease of 99.8%. The aged CCRT still had a near-perfect effect on the PN, with a decrease of 99.7%. In terms of the PM emission factor, it reached 20.87 mg/km for the bus without CCRT. When the bus was equipped with the fresh CCRT, the PM emission factor fell to 0.54 mg/km, with a decrease of 97.4%. However, for the aged CCRT, the reduction effect on the PM emission

factor declined slightly, with a decrease of 93.9%. This is because the aging of the CCRT weakens the oxidation of soluble organic fractions (SOF). On the other hand, the aged upstream DOC leads to a weakened NO oxidation ability. Therefore, the downstream CDPF is short of having enough NO_2 to oxidize the captured particles.

To understand the differences in the overall PSD of the bus before and after CCRT use, and the effect of the aged CCRT on the PSD, the number-weighted PSDs of the bus with the fresh and the aged CCRT are given in **Fig. 9**. **Fig. 9** shows that the PN concentration decreased significantly, and the PSD peaks shifted to smaller particle sizes after using CCRT. This is because the catalyst in the DOC and CDPF oxidized the SOF adsorbed on the particulate matter, leading to a reduction in the size of particles. (Young et al., 2012). The peaks of the nucleation (< 50 nm) and accumulation (> 50 nm) mode particle number concentrations were near 19.1 and 165.5 nm, respectively, before the bus started using CCRT. After the installation of the CCRT, the nucleation and accumulation mode peaks shifted to 12.4 and 80.6 nm respectively, and the proportion of the nucleation mode particles decreased from 98% to 66%. The main reason is that the CCRT can oxidize most of the SOF in the particulates, which may be measured as nucleation mode particles by EEPS (Zhang et al., 2018b). The aged CCRT had no obvious effect on the PSD, but its effect on PN reduction was slightly inferior to that of the fresh CCRT, and the proportion of nucleation mode particles presented a rising trend and reached 71%, which can be attributed to the deterioration of the catalyst of the CCRT, causing a reduced SOF oxidation activity (Tartakovsky et al., 2015; Sandra et al., 2016; Zhou et al., 2018). In addition, the accumulated ash in the aged CDPF also weakened the oxidation activity of the catalyst by covering the active sites of the catalyst (Yamazaki et al., 2016).

2.2 Activity evaluation of samples

The conversion rates of CO and C_3H_8 and the NO_2 production rates of the fresh and aged CCRT catalyst as a function of temperature are shown in **Fig. 10.** The conversion rates of CO and C_3H_8 and the NO_2 production rates increased with temperature. The CO conversion rate of the fresh catalyst sample was higher than that of the aged one when the temperature was < 240℃; then the CO conversion rates of fresh and aged catalyst samples were equivalent, and both reached approximately 100%. The C_3H_8 conversion rates were very low (< 10%) both for the fresh and the aged catalyst samples when the temperature was ≤ 300℃ due to competitive adsorption with CO (Goto et al., 2014), and then they increased rapidly with temperature. Through the whole temperature range, the C_3H_8 conversion rate of the fresh catalyst sample was always higher than that of the aged catalyst sample, and when the

temperature reached 500℃, the C_3H_8 conversion rate of fresh catalyst sample was 90%. However, for the aged catalyst sample, the conversion rate of C_3H_8 was only 50%. The NO_2 production rates of the fresh and aged catalyst samples increased with temperature and showed a similar trend. It can be seen that there were no peaks for NO_2 production at ~ 400℃, caused by the chemical equilibrium limitation (Tang et al., 2014); the main reason is that the presence of CO and C_3H_8 inhibited NO oxidation (Hauff et al., 2012). The NO_2 production rate of the fresh catalyst sample was higher than that of the aged one. When the temperature was 500℃, the NO_2 production rate of the fresh catalyst sample was 24.5%, while for the aged sample, the NO_2 production rate was 16.1%. In terms of the catalyst light-off temperature, it can be seen that the T_{50} (the temperature of 50% conversion) for CO of the fresh catalyst sample was 115℃, while for the aged sample, T_{50} was about 210℃. In terms of the light-off characteristics of C_3H_8, the T_{50} was 410℃ for the fresh sample, but for the aged sample, the T_{50} increased to 500℃. For NO oxidation, the T_{15} (the temperature of 15% conversion) for the fresh catalyst sample was 240℃, while for the aged sample, T_{15} increased to 440℃. The aged CCRT catalyst resulted in higher light-off temperatures because the crystallinity of the catalyst sample increased after aging, which inhibits the migration and activation of the surface oxygen and reduces the dispersion of Pt and Pd on the surface of the support, resulting in a reduction of active sites (Chen et al., 2015).

2.3 Active element analysis by XPS

Fig. 11 gives the mole percentages of Pt^{2+} and Pt^{4+} on the catalyst samples before and after aging. It can be observed that the mole percentages of Pt^{2+} and Pt^{4+} were 0.67 and 0.70 mol.% for the fresh catalyst sample. Compared with the fresh one, the mole percentages of Pt^{2+} and Pt^{4+} of the aged catalyst sample decreased by 70.27 and 67.52%, and they reached 0.20 and 0.23 mol.%, respectively. The declining Pt^{2+} and Pt^{4+} components reflected that high temperature resulted in sintering of the active element, which reduced the number of active sites (Wiebenga et al., 2012).

3 Conclusions

The reduction effect of a CCRT on the main exhaust emissions from an urban diesel bus was investigated based on a heavy chassis dynamometer, and the durability of this effect was also studied. In addition, a laboratory activity evaluation and XPS evaluation were applied to characterize the catalyst changes of the aged CCRT. The main conclusions are listed below:

(1) The fresh CCRT reduced the CO by 71.5% and the THC by 88.9%, while for the aged CCRT, the conversion of CO and THC declined to 25.2% and 55.1%, respectively. The use of the CCRT promoted the NO oxidation, but this oxidation ability was weakened after aging.

(2) The fresh CCRT could reduce more than 97% of the PM and almost 100% of the PN, but an obvious reduction in the PM trapping efficiency was observed after aging. The use of a CCRT shifted the peaks of the PSD to a smaller size and decreased the proportion of nucleation mode particles, but for the aged CCRT, its effect on nucleation mode PN reduction was slightly inferior to that of the fresh CCRT.

(3) The T_{50} values for CO and C_3H_8 of the aged catalyst sample increased by 95 and 90℃ respectively compared with the fresh one, and the T_{15} of the NO_2 production for the aged CCRT was 200℃ higher than that of the fresh one. Meanwhile, the aged CCRT showed reductions in Pt^{2+} and Pt^{4+} mole percentages by 70.27 and 67.52 %. The increase in the light-off temperatures and decrease of Pt^{2+} and Pt^{4+} components of the aged CCRT are the direct reasons for the CCRT deterioration.

Acknowledgments

This work was supported by the National Key Research and Development Program of China (No. YS2017ZY020019), Research Project of Shanghai Committee of Science and Technology (No. 18DZ1202900) and the China Scholarship Council (No. 201806260133).

References

Auvray, X., Pingel, T., Olsson, E., Olsson, L., 2013. The effect gas composition during thermal aging on the dispersion and NO oxidation activity over Pt/Al_2O_3 catalysts. Appl. Catal. B-Environ. 129, 517-527.

Caliskan, H, Mori, K., 2017. Environmental, enviroeconomic and enhanced thermodynamic analyses of a diesel engine with diesel oxidation catalyst (DOC) and diesel particulate filter (DPF) after treatment systems. Energy 128, 128-144.

Chen, X., Cheng, Y., Seo, C.Y., Schwank, J.W., McCabe, R.W., 2015. Aging, re-dispersion, and catalytic oxidation characteristics of model Pd/Al_2O_3 automotive three-way catalysts, Appl. Catal B-Environ. 163, 499-509.

Fleischman, R., Amiel, R., Czerwinski, J., Mayer, A., Tartakovsky, L., 2018. Buses retrofitting with diesel particle filters: Real-world fuel economy and roadworthiness test considerations. J. Environ. Sci. 67, 273-286.

Gilpin, G., Hanssen, O. J., Czerwinski, J., 2014. Biodiesel's and advanced exhaust aftertreatment's combined effect on global warming and air pollution in EU road-freight transport. J. Clean. Prod. 78, 84-93.

Goto, Y., Kato, N., Kawashima, S., Hayashi, Y., Goto, H., Hori, M., 2014. Applicable diesel oxidation catalyst for multi-diesel exhaust system. SAE International Journal of Fuels and Lubricants 7(2), 496-502.

Guan, B., Zhan, R., Lin, H., Huang, Z., 2015. Review of the state-of-the-art of exhaust particulate filter technology in internal combustion engines. J. Environ. Manage. 154, 225-258.

Guardiola, C., Pla, B., Piqueras, P., Mora, J., Lefebvre, D., 2017. Model-based passive and active diagnostics strategies for diesel oxidation catalysts. Appl. Therm. Eng. 110, 962-971.

Hauff, K., Tuttlies, U., Eigenberger, G., Nieken, U., 2010. A global description of DOC kinetics for catalysts with different platinum loadings and aging status. Appl. Catal B-Environ. 100, 10-18.

Hauff, K., Tuttlies, U., Eigenberger, G., Nieken, U., 2012. Platinum oxide formation and reduction during NO oxidation on a diesel oxidation catalyst-Experimental results. Appl. Catal. B-Environ. 123, 107-116.

He, C., Li, J., Ma, Z., Tan, J., Zhao, L., 2015. High NO_2/NOx emissions downstream of the catalytic diesel particulate filter: An influencing factor study. J. Environ. Sci. 35, 55-61.

Honkanen, M., Hansen, T.W., Jiang, H., Kärkkäinen, M., Huuhtanen, M., Heikkinen, O., et al., 2017. Electron microscopic studies of natural gas oxidation catalyst - Effects of thermally accelerated aging on catalyst microstructure. J. Catal. 349, 19-29.

Johns, T.R., Goeke, R.S., Ashbacher, V., Thüne, P.C., Niemantsverdriet, J.W., 2015. Relating adatom emission to improved durability of Pt-Pd diesel oxidation catalysts. J. Catal. 328, 151-164.

Jung, S., Lim, J., Kwon, S., Jeon, S., Kim, J., Lee, J., et al., 2017. Characterization of particulate matter from diesel passenger cars tested on chassis dynamometers. J. Environ. Sci. 54, 21-32.

Kim, H., Sung, Y, Jung, K., Choi, B., Lim, M.T., 2008. Size distributions and number concentrations of particles from the DOC and CDPF. J. Mech. Sci. Technol. 22, 1793-1799.

Kolli, T., Kanerva, T., Huuhtanen, M., Vippola, M., Kallinen, K., Kinnunen, T., et al., 2010. The activity of Pt /Al_2O_3 diesel oxidation catalyst after sulphur and calcium treatments. Catal. Today 154, 303-307.

Li, J., Szailer, T., Watts, A., Currier, N., Yezerets, A., 2012. Investigation of the impact of real-world aging on diesel oxidation catalysts. SAE International Journal of Engines 5(3), 985-994.

Liu, J., Ge, Y., Wang, X., Hao, L., Tan, J., Peng, Z., et al., 2017. On-board measurement of particle numbers and their size distribution from a light-duty diesel vehicle: Influences of VSP and altitude. J. Environ. Sci. 57, 238-248.

Lou, D.M., He, N., Tan, P.Q., Hu, Z.Y., 2016. Effect of DOC/CCRT aging on gaseous emission characteristics of an in-used diesel engine bus. Environmental Science 37(6), 2059-2064.

Luo, J.Y., Kisinger, D., Abedi, A., Epling, W.S., 2010. Sulfur release from a model Pt/Al_2O_3 diesel oxidation catalyst: Temperature-programmed and step-response techniques characterization. Appl. Catal. A-Gen. 383, 182-191.

Matam, S. K., Kondratenko, E. V., Aguirre, M. H., Hug, P., Rentsch, D., Winkler, A., et al., 2013. The impact of aging environment on the evolution of Al_2O_3 supported Pt nanoparticles and their NO oxidation activity. Appl. Catal. B-Environ. 129, 214-224.

Orihuela, M.P., Gómez-Martín, A., Miceli, P., Becerra, J.A., Chacartegui, R. Fino, D., 2018. Experimental measurement of the filtration efficiency and pressure drop of wall-flow diesel particulate filters (DPF) made of biomorphic Silicon Carbide using laboratory generated particles. Appl. Therm. Eng. 131, 41-53.

Sandra, F., Ballestero, A., Tsampas, M. N., Vernoux, P., Balan, C., Iwamoto, Y., et al., 2016. Silicon carbide-based membranes with high soot particle filtration efficiency, durability and catalytic activity for CO/HC oxidation and soot combustion. J. Membrane. Sci. 501, 79-92.

Shen, X., Shi, J., Cao, X., Zhang, X., Zhang, W., Wu, H., et al., 2018. Real-world exhaust emissions and fuel consumption for diesel vehicles fueled by waste cooking oil biodiesel blends. Atmos. Environ. 191, 249-257.

Shen, X., Yao, Z., Zhang, Q., Wagner, D. V., Huo, H., Zhang, Y., et al., 2015. Development of database of real-world diesel vehicle emission factors for China. J. Environ. Sci. 31, 209-220.

Tang, T., Zhang, J., Cao, D., Shuai, S., Zhao, Y., 2014. Experimental study on filtration and continuous regeneration of a particulate filter system for heavy-duty diesel engines. J. Environ. Sci. 26(12), 2434-2439.

Tartakovsky, L., Baibikov, V., Comte, P., Czerwinski, J., Mayer, A., Veinblat, M., et al., 2015. Ultrafine particle emissions by in-use diesel buses of various generations at low-load regimes. Atmos. Environ. 107, 273-280.

Wiebenga, M. H., Kim, C. H., Schmieg, S. J., Oh, S. H., Brown, D. B., Kim, D. H., et al., 2012. Deactivation mechanisms of Pt/Pd-based diesel oxidation catalysts. Catal. Today 184(1), 197-204.

Yamazaki, K., Sakakibara, Y., Daido, S., Okawara, S., 2016. Particulate matter oxidation over ash-deposited catalyzed diesel particulate filters. Top. Catal. 59(10-12), 1076-1082.

Young, L. H., Liou, Y. J., Cheng, M. T., Lu, J. H., Yang, H. H., Tsai, Y. I., et al., 2012. Effects of biodiesel, engine load and diesel particulate filter on nonvolatile particle number size distributions in heavy-duty diesel engine exhaust. J. Hazard. Mater. 199, 282-289.

Zhang, Y., Lou, D., Tan, P., Hu, Z., 2018a. Experimental study on the durability of biodiesel-powered engine equipped with a diesel oxidation catalyst and a selective catalytic reduction system. Energy 159, 1024-1034.

Zhang, Y, Lou, D, Tan, P, Hu, Z., 2018b. Experimental study on the particulate matter and nitrogenous compounds from diesel engine retrofitted with DOC+CDPF+SCR. Atmos. Environ. 177, 45-53.

Zhang, Y., Lou, D., Tan, P., Liu, J., 2017. Purification performance and deterioration rule of catalyzed diesel particulate filter. Journal of Tongji University (Natural Science) 45 (12), 1866-1872.

Zhou, H., Zhao, H., Yin, Z., Feng, Q., Zhou, M., Li, J., et al., 2018. Deterioration characteristic of catalyzed DPF applied on diesel truck durable ageing. In: WCX™18: SAE World Congress. Detroit, USA. Apr 10-12.

List of tables

Table 1 Specifications of the diesel oxidation catalyst (DOC) and catalyzed diesel particulate filter (CDPF)

Parameter	Feature/value	
	DOC	CDPF
Substrate	FeCrAl	Cordierite
Cell density (cell/cm^2)	62	31

Wall thickness (mm)	0.06	0.35
Porosity	None	55%
Catalyst	Pt/Pd/Rh	Pt/Pd/Rh
Catalyst load (g/L)	1.94	0.88
Precious metal ratio	10:1:0	10:2:1
Coatings	γ-Al_2O_3	γ-Al_2O_3

List of figures

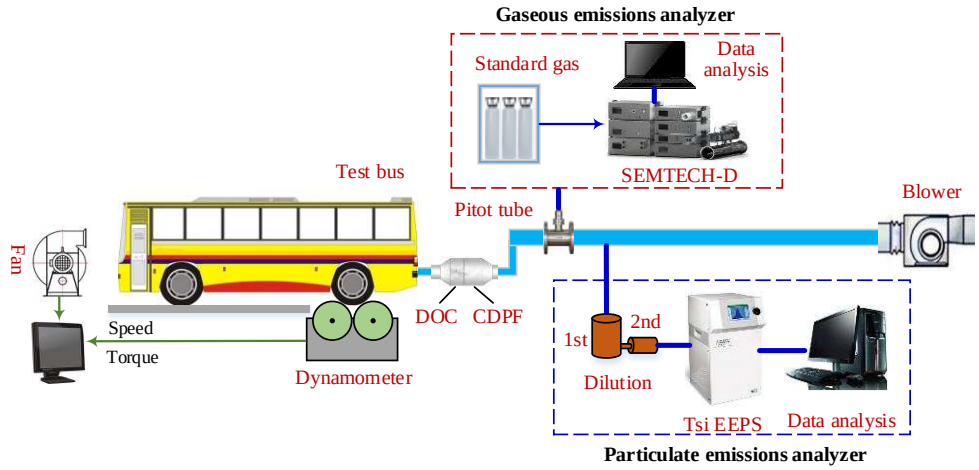

Fig. 1 Schematic diagram of the experimental system. EEPS: engine exhaust particle sizer; DOC: diesel oxidation catalyst; CDPF: catalyzed diesel particulate filter.

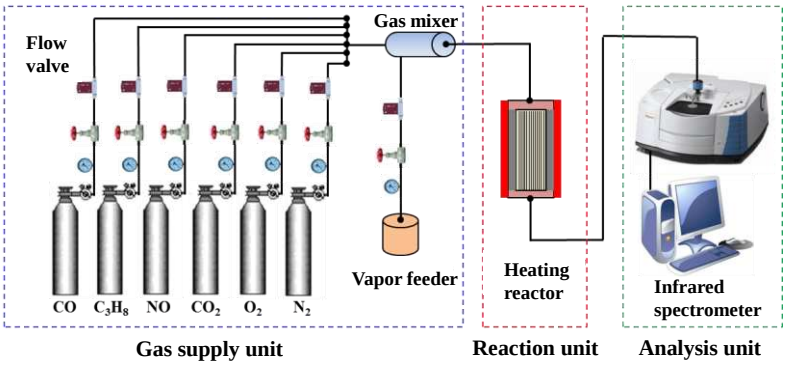

Fig. 2 Schematic diagram of the temperature-programmed reduction (TPR) test system.

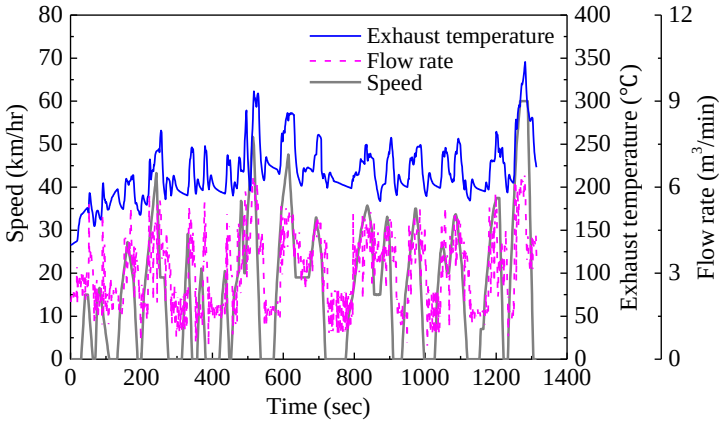

Fig. 3 Exhaust temperature and exhaust flow rate during the Chinese city bus cycle (CCBC) driving cycle.

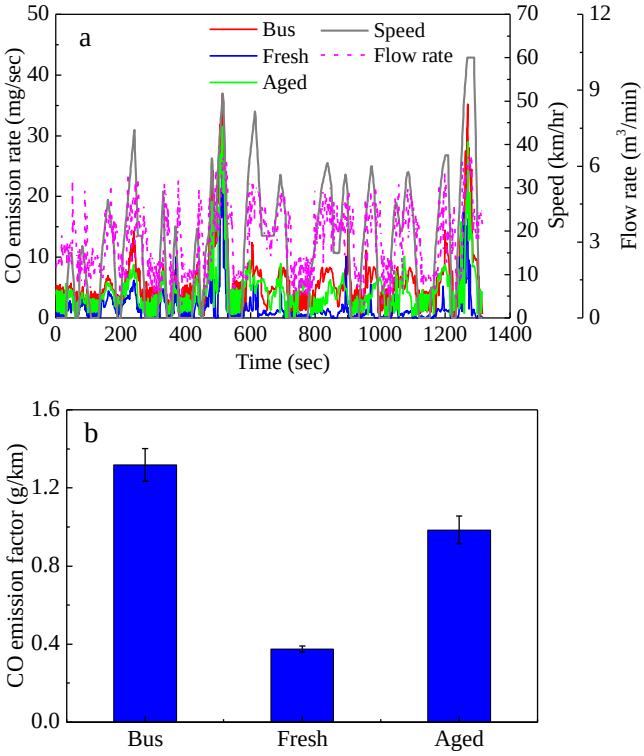

Fig. 4 (a) CO emission rate and (b) CO emission factors of the fresh and aged catalyzed continuously regenerating trap (CCRT).

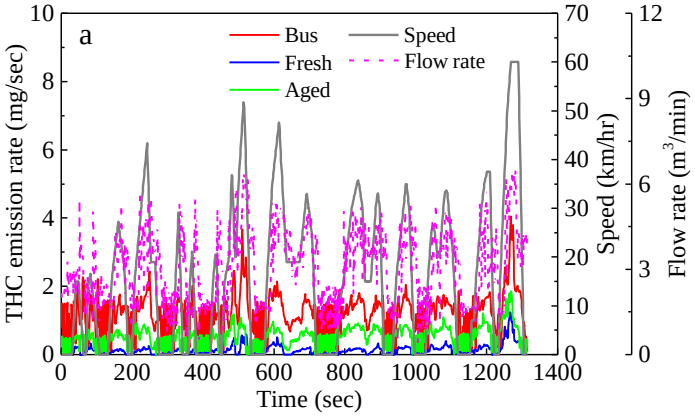

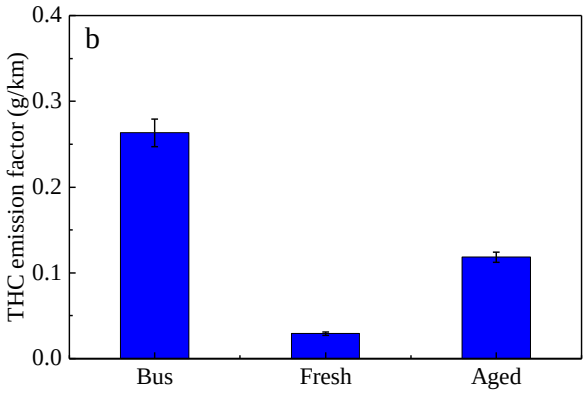

Fig. 5 (a) THC emission rate and (b) THC emission factors of the fresh and aged CCRT. THC: total hydrocarbons.

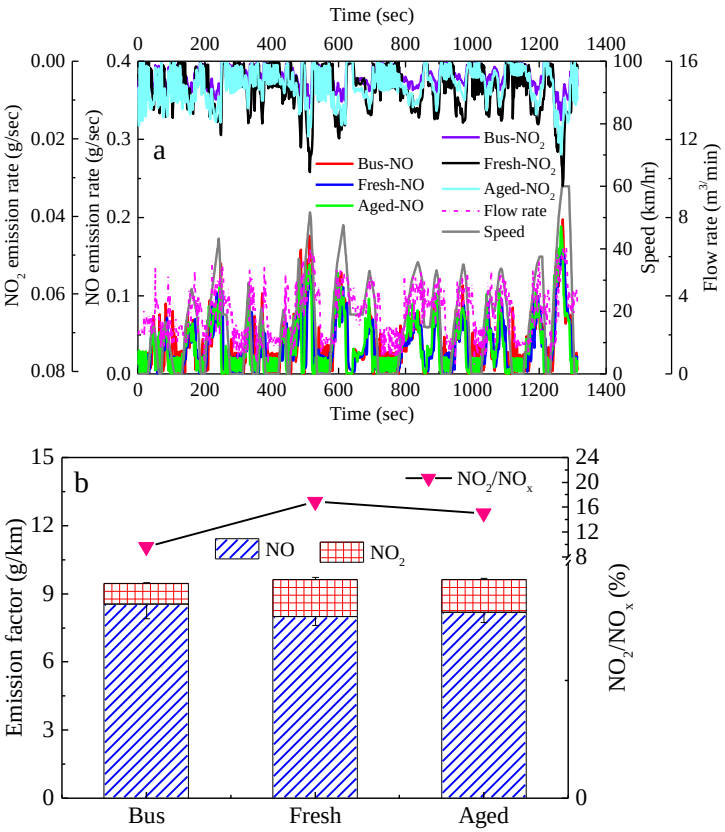

Fig. 6 (a) NO/NO_2 emission rates and (b) NO/NO_2 emission factors of the fresh and aged CCRT.

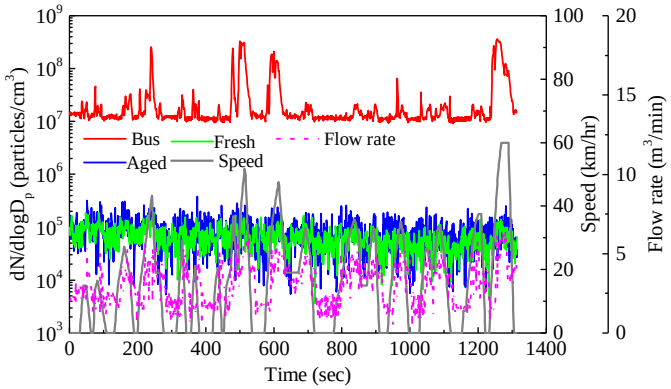

Fig. 7 Particle number (PN) concentration emissions of the fresh and aged CCRT.

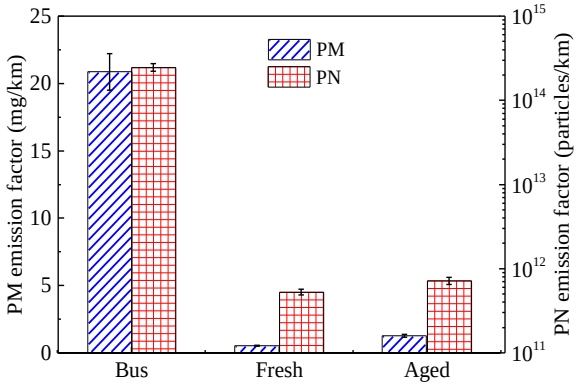

Fig. 8 Particle mass (PM) and PN emission factors of the bus, fresh and aged CCRT.

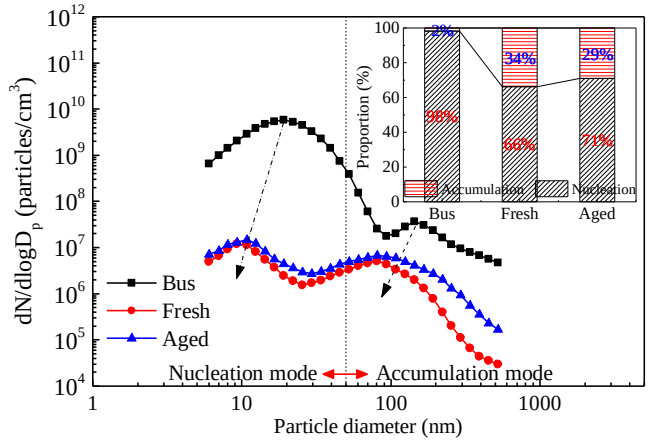

Fig. 9 Particle size distributions and (inset) particle proportions of the fresh and aged CCRT.

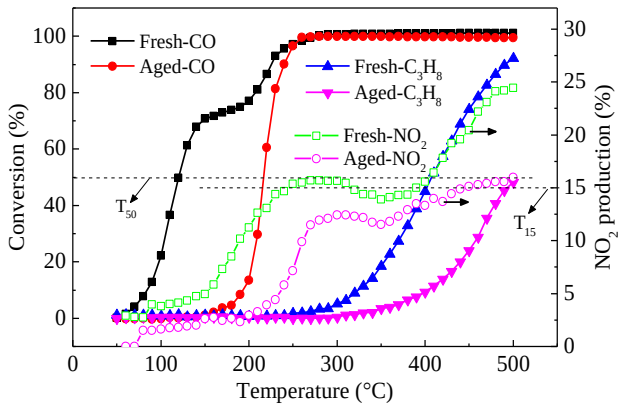

Fig. 10 CO, C_3H_8 conversion rates and NO_2 production rate with temperature. T_{50}: the temperature of 50% conversion; T_{15}: the temperature of 15% conversion.

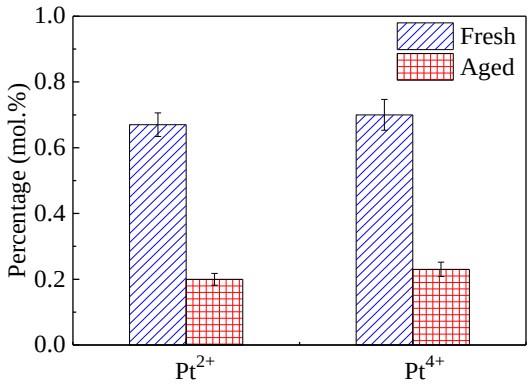

Fig. 11 Active element analysis of the fresh and aged catalyst samples.